

## Article

# Facile Synthesis of MXene/MnO<sub>2</sub> Nanocomposites for Efficient Removal of Radionuclide Uranium

Ling Wang<sup>1</sup> and Yi-Lin Liu<sup>1,2,\*</sup> <sup>1</sup> College of Chemistry and Chemical Engineering, University of South China, Hengyang 421001, China<sup>2</sup> College of Mechanical Engineering, University of South China, Hengyang 421001, China

\* Correspondence: liuyilin@usc.edu.cn

**Abstract:** The efficient removal of radionuclide uranium is crucial for sustainable nuclear energy and achieving a zero-carbon loop. In this study, we synthesized MXene/MnO<sub>2</sub> nanocomposites and evaluated their ability to adsorb and reduce uranium. The results showed that the nanocomposites achieved a uranium removal rate of 99% and an adsorption capacity of 696 mg/g. Adsorption experiments were conducted under different conditions, including pH, cation, anion, and humic acid, and the uranium removal rate by the composite remained high at 91%, 70%, and 60% under the influence of pH = 4.97, 1.0 mM CaCl<sub>2</sub>, and 20 mg/L humic acid, respectively. The XRD and SEM analyses revealed that the uranium element was removed by the reduction and fixation of the composite material. These findings indicate that the MXene/MnO<sub>2</sub> composite is an effective adsorption cleaning agent for the purification of radioactive nuclear wastewater, which has significant implications for pollution control.

**Keywords:** MXene; MnO<sub>2</sub>; nanocomposites; adsorption performance; uranium



**Citation:** Wang, L.; Liu, Y.-L. Facile Synthesis of MXene/MnO<sub>2</sub> Nanocomposites for Efficient Removal of Radionuclide Uranium. *Crystals* **2023**, *13*, 804. <https://doi.org/10.3390/cryst13050804>

Academic Editors: Helmut Cölfen and Volodymyr Bon

Received: 26 April 2023

Revised: 9 May 2023

Accepted: 9 May 2023

Published: 11 May 2023



**Copyright:** © 2023 by the authors. Licensee MDPI, Basel, Switzerland. This article is an open access article distributed under the terms and conditions of the Creative Commons Attribution (CC BY) license (<https://creativecommons.org/licenses/by/4.0/>).

## 1. Introduction

The rapid development of advanced nuclear energy and renewable energy technologies, as well as the gradual replacement of fossil energy, highlights the significance of effective disposal of radioactive nuclear waste pollutants for human health and the safety of the living environment [1–3]. Although the development and utilization of nuclear energy promote economic and social development, it also leads to the aggravation of radioactive pollution [4–7]. The production of uranium tailings and waste rock in mining and nuclear energy production release radionuclides and toxic elements through rain leaching and weathering, resulting in a rapid increase in the discharge of radioactive wastewater containing uranium [8–10].

Uranium is a radioactive and chemically toxic element, which exists as UO<sub>2</sub><sup>2+</sup> in an oxidizing acidic solution, making it easier to migrate. If released into the environment without effective treatment, it can cause harm to human health and the ecosystem. Therefore, immobilizing uranium is crucial to reduce its migration and prevent environmental damage [11–13]. Organic uranyl minerals can exist stably under natural conditions in natural uranium ores and uranium-contaminated soil and sediment. Based on the new ecological restoration concept of uranium pollution returning to natural minerals, studying the principle and technology of stability control of uranyl and phosphate mineralization is essential to blockage and control of uranium pollution in wastewater, ensuring the safe development of nuclear energy and the construction of ecological civilization [14–18].

MXene materials have been widely studied for their excellent properties, including excellent catalytic, storage, mechanical, and magnetic properties, as well as selective properties for a variety of ions [19–23]. Researchers worldwide have prepared MXene-loaded composite materials, such as zero-valent iron and copper, and tested their efficacy for storing energy in battery capacitors and removing harmful ions or organic matter from the ecological environment by adsorption and reduction [24–30].

In this paper, we use the HF in-situ etching method to prepare MXene and then prepare MXene/MnO<sub>2</sub> composites by ultrasonication and continuous centrifugation of a mixed solution of MXene and potassium permanganate. Subsequently, we test the removal efficiency of MXene/MnO<sub>2</sub> composites for uranium-containing radionuclides under the influence of different environmental factors. This study aims to determine whether the MXene/MnO<sub>2</sub> composites can be widely used in the cleaning and purification of uranium-containing radioactive waste liquid.

## 2. Experimental Detail

### 2.1. Reagents and Chemicals

The following chemical reagents were used in this experiment: titanium aluminum carbide (Ti<sub>3</sub>AlC<sub>2</sub>) powder for preparing MXene materials, lithium fluoride (LiF), hydrochloric acid (HCl), uranyl nitrate (UO<sub>2</sub>(NO<sub>3</sub>)<sub>2</sub>·6H<sub>2</sub>O), pure water (for cleaning beakers, measuring cylinders and other equipment), ultrapure water (for preparing solutions), potassium permanganate (KMnO<sub>4</sub>), sodium chloride (NaCl), calcium chloride (CaCl<sub>2</sub>·2H<sub>2</sub>O), potassium chloride (KCl), copper chloride (CuCl<sub>2</sub>·2H<sub>2</sub>O), cobalt nitrate (Co(NO<sub>3</sub>)<sub>2</sub>·6H<sub>2</sub>O), nickel nitrate (Ni(NO<sub>3</sub>)<sub>2</sub>·6H<sub>2</sub>O), ferrous sulfate (FeSO<sub>4</sub>·7H<sub>2</sub>O), ferric chloride (FeCl<sub>3</sub>·6H<sub>2</sub>O), sodium nitrate (NaNO<sub>3</sub>), sodium sulfate (Na<sub>2</sub>SO<sub>4</sub>), sodium bicarbonate (NaHCO<sub>3</sub>), ammonium fluoride (NH<sub>4</sub>F), and humic acid from Sinopharm Chemical Reagent Co., Ltd. (Shanghai, China).

### 2.2. Preparation of MXene/MnO<sub>2</sub> Composite

- (1) In a beaker, 2 g lithium fluoride (LiF) and 22.5 mL hydrochloric acid (HCl) were slowly added to 7.5 mL ultrapure water (deionized water) solution at room temperature. The mixture was then placed on a magnetic stirrer and covered with plastic wrap. Then, 1 g of Ti<sub>3</sub>AlC<sub>2</sub> powder was added to the mixed solution over a period of 30 min. The obtained solution was put into a hydrothermal reaction kettle and placed in a water bath. The reaction was kept on the stirrer for 24–48 h under the water bath at 35 °C.
- (2) After stirring in the water bath, the material obtained in step (1) was poured into several different centrifuge tubes. Ultrapure water was added to these tubes, and the tubes were shaken well to ensure that the quality of each centrifuge tube was the same (around 0.5 mg). These centrifuge tubes were then centrifuged with a high-speed centrifuge at 3500 r/min for 5 min. The centrifuged material and its supernatant were discarded, and the precipitated part was retained. This process was repeated 6 or 7 times until the pH of the obtained supernatant was around 6.
- (3) The material obtained by centrifugation in step (2) was poured into a centrifuge tube and 20 mL ultrapure water was added. The tube was closed, and the material was shaken by hand for 2 h. Then, 20 mL ultrapure water was added, and the supernatant was obtained after centrifugation at 3500 r/min for 30 min. Next, 20 mL ultrapure water was added to the precipitate, shaken by hand for 30 min, and then, 20 mL ultrapure water was added. The supernatant was obtained after centrifugation at 5000 r/min for 20 min. The precipitate was then taken and added to 20 mL ultrapure water, which was then ultrasonically treated through an ultrasonic cleaner for 25 min. Next, 20 mL ultrapure water was added, and the solution was centrifuged at 5000 r/min for 20 min to obtain the supernatant.
- (4) The supernatant liquid obtained in step (3) was frozen in a refrigerator or under the condition of liquid nitrogen. It was then put into a centrifuge tube, opened, and placed in an atmosphere of an inert gas such as nitrogen to dry. The desired MXene nanomaterials were obtained by drying them at 60 °C for about 24 h. The MXene material was stored in a refrigerator for later use.
- (5) To prepare the MXene/MnO<sub>2</sub> composites, several hydrothermal reactor inner liners were taken, and 70 mL ultrapure water was measured through a graduated cylinder. Ultrapure water was added to the reactor, and 20 mg MXene was weighed with an electronic analytical balance and slowly added to the reaction kettle to obtain a

mixed solution. The lid of the reaction kettle was fastened, and it was put into an ultrasonic cleaner for about 10 min. Then, the magnet was added to the solution, and the reaction kettle was placed on the magnetic stirrer and stirred at a speed of about 500 r/min for 7–8 min. Next, 25 mg potassium permanganate powder was weighed out using an electronic analytical balance and slowly added to the stirring solution. After completing the stirring process, the magnet was removed, and the lid of the reactor was securely fastened. Next, the reactor was placed into the hydrothermal reactor and tightened before inserting it into an oven at a temperature of 120 °C for 4 h. After the hydrothermal treatment was completed, the reactor was removed and the supernatant solution was poured out. Next, the sedimentation part of the lower layer was carefully poured into multiple centrifuge tubes, and ultrapure water was added to the tubes to ensure that the mass difference between the tubes was less than 0.5 mg. Then, the tubes were centrifuged using a high-speed centrifuge for 10 min at a rotational speed of 6000 r/min. After centrifugation, the precipitates were transferred to a drying oven, and the lid was opened. The material was dried at 60 °C for 24 h to obtain the desired powder of MXene/MnO<sub>2</sub> composites.

### 2.3. Batch Adsorption Experiments

Several 50 mL beakers were used in this experiment. First, 45 mL ultrapure water was measured with a graduated cylinder and added to each beaker. Nitrogen gas was then passed through the solution for 30 min. Next, 5 mg of the previously prepared MXene/MnO<sub>2</sub> composites powder was added to the solution, and the beaker mouth was sealed with plastic wrap. The beaker was then sonicated in an ultrasonic cleaner for 15 min. Nitrogen gas was continuously passed through the solution to prepare for adsorption. To initiate adsorption, 5 mL of 200 mg/L U(VI) solution was added to the beaker solution that was purged with nitrogen. The solution was then mixed and left to react for 10 s, 20 s, 40 s, 1 min, 2 min, and 4 min. After each reaction time, a small amount of the reacting solution was immediately taken and transferred to microcentrifuge tubes using disposable sterile syringes and filter heads. The centrifuge tubes were then capped and set aside for later use.

Samples were obtained after adsorption of U(VI) solution with different concentration. Specifically, 10 mL, 20 mL, 30 mL, 37.5 mL, and 50 mL of 200 mg/L U(VI) solution were added to separate beakers and repeated adsorption and reduction experiments were performed using the above method.

To test the uranium concentration, we used a WGJ-III microuranium analyzer to determine microuranium in liquid samples by ultraviolet fluorescence method. Uranium exists in liquid as uranyl ion (UO<sub>2</sub>)<sup>2+</sup>. By adding a special J-22 uranium fluorescence enhancer, the uranyl ion is complex into a single complex with high fluorescence efficiency. The complex is excited by UV pulses to produce fluorescence at wavelengths of 500 nm, 522 nm, and 546 nm. This fluorescence intensity represents the amount of uranium in the sample. A rectangular cuvette that was transparent on all sides was used. First, 4.9 mL of ultrapure water was added to the cuvette using a pipette. Next, 1.5 mL of trace uranium fluorescence enhancer and 1 mL of the sample from the centrifuge tube were added to the cuvette, and the mixture was stirred evenly with a glass rod. The cuvette was then placed in a micro uranium analyzer to measure the uranium concentration.

The adsorption capacity  $q$  (mg/g) and removal rate  $E$  (%) of U(VI) were calculated using the following formulas [31–33]:

$$q = (C_0 - C)/m \times V \quad (1)$$

$$E = (C_0 - C)/C_0 \times 100\% \quad (2)$$

In the formula,  $C_0$  (mg/L) is the concentration before the adsorption of U(VI) in the solution;  $C$  (mg/L) is the concentration after the adsorption of U(VI) in the solution;  $m$ (g) is the mass of the solid-phase adsorbent; and  $V$ (L) is the volume of the solution [9–12].

## 2.4. Characterization

The morphologies and chemical compositions of  $\text{Ti}_3\text{C}_2\text{T}_x/\text{MnO}_2$  were analyzed using a scanning electron microscope (SEM, Hitachi S-4800). X-ray diffraction (XRD) measurement was carried out on a Bruker D8 Advance X-ray diffraction instrument (Cu  $K\alpha$  radiation,  $\lambda = 1.5406 \text{ \AA}$ ) with a step size of  $0.02^\circ$  and a diffraction angle ( $2\theta$ ) ranging from  $3^\circ$  to  $70^\circ$ .

## 3. Results and Discussion

### 3.1. Characterization of MXene/ $\text{MnO}_2$ Composites

To analyze the microscopic morphology of the prepared composites, the MXene/ $\text{MnO}_2$  composites were characterized and analyzed by SEM. The  $\text{Ti}_3\text{AlC}_2$  powder nanoflakes were first etched with lithium fluoride and hydrochloric acid, resulting in a change in morphology that indicated successful etching of the Al atoms. The  $\text{MnO}_2$  was uniformly dispersed on the nanosheets of  $\text{Ti}_3\text{C}_2$ , indicating the strong surface adsorption capacity of the MXene/ $\text{MnO}_2$  composites and efficient adsorption and reduction of U(VI). Figure 1a shows a  $2000\times$  magnified SEM image of  $\text{Ti}_3\text{AlC}_2$  powder nanoflakes, which are dispersed into irregular sheets with crack-shaped boundaries. The lateral dimensions of these flakes are about  $2 \mu\text{m}$ . Figure 1b shows relatively large voids in the middle of the morphology of the material, which are caused by the extraction of the second layer in the middle of the three-layer atoms of the  $\text{Ti}_3\text{AlC}_2$  nanosheet layer. Figure 1c shows an SEM image of the MXene/ $\text{MnO}_2$  composite at 10,000 times magnification, where round particles of  $\text{MnO}_2$  are densely arranged on the surface of the MXene material. The characteristics of these  $\text{MnO}_2$  round particles are that they are uniformly dispersed on the surface of the MXene material, providing relatively excellent adsorption capacity due to their dense and uniform characteristics. Figure 1d shows the SEM image formed at a magnification of 20,000 times, which displays the detailed structure and morphology of the MXene/ $\text{MnO}_2$  composite. This structure provides active sites for the adsorption-reduction reaction with different and strong selectivities for different ion adsorption. These active sites can be more easily used in radioactive nuclear wastewater with a variety of competing ions, allowing the MXene/ $\text{MnO}_2$  composites can effectively adsorb uranium nuclides under the interference of different ecological environment conditions.

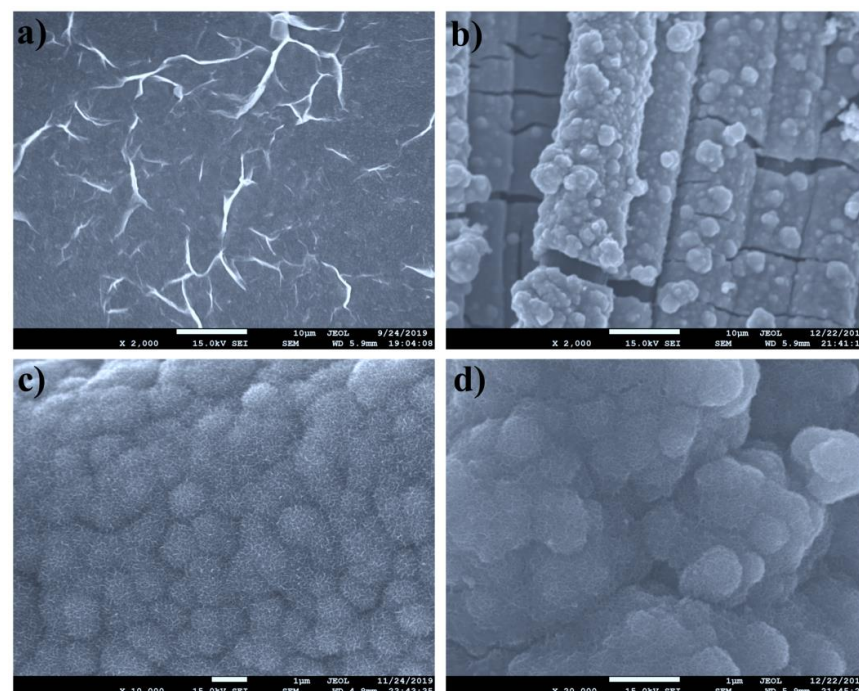


**Figure 1.** (a) SEM images of  $\text{Ti}_3\text{C}_2$  nanosheets, (b–d) SEM images of MXene/ $\text{MnO}_2$  composites.

Figure 2 shows the XRD patterns of  $\text{Ti}_3\text{AlC}_2$ , MXene, and MXene/ $\text{MnO}_2$  composites. It is evident that  $\text{Ti}_3\text{AlC}_2$  material shows multiple diffraction peaks at around  $2\theta = 40^\circ$ , while there is no corresponding peak in the XRD pattern of MXene and MXene/ $\text{MnO}_2$  composites. This observation indicates that the Al element in  $\text{Ti}_3\text{AlC}_2$  has been successfully etched away by the in-situ etching method by adding LiF and HCl.

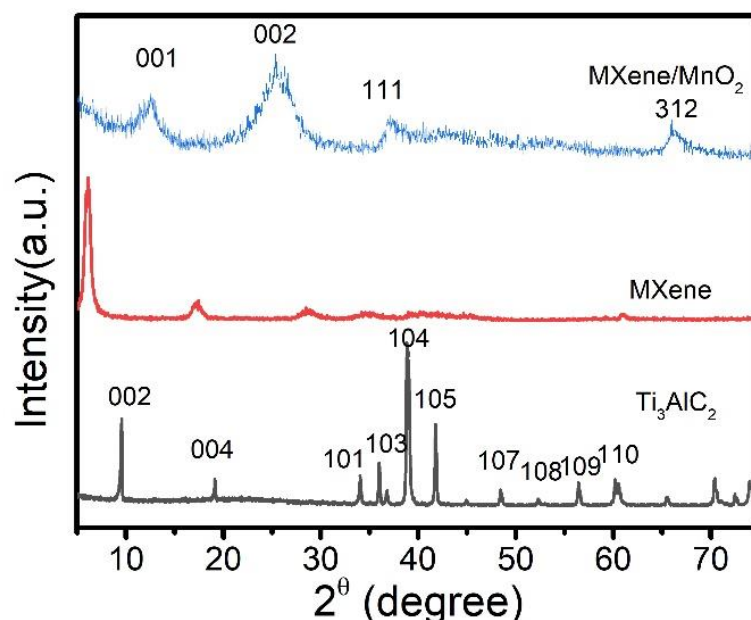
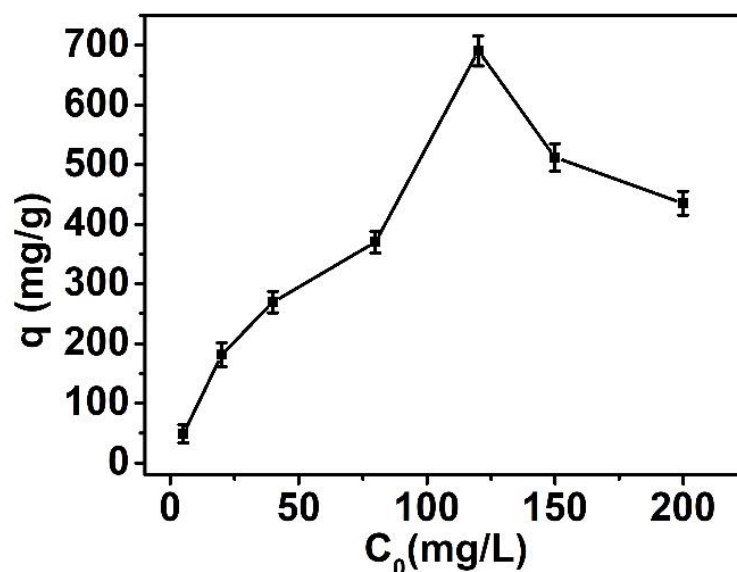


Figure 2. XRD patterns of  $\text{Ti}_3\text{AlC}_2$ , MXene, and MXene/ $\text{MnO}_2$  composites.

Furthermore,  $\text{Ti}_3\text{AlC}_2$  exhibits a (002) diffraction peak at  $2\theta = 10^\circ$ , which is also observed in the XRD pattern of MXene, confirming the successful preparation of MXene material. In the XRD pattern of MXene/ $\text{MnO}_2$  composite, the (002) diffraction peak of MXene is still visible, in addition to three new diffraction peaks at  $2\theta = 12.1^\circ$ ,  $2\theta = 36.3^\circ$ , and  $2\theta = 65.2^\circ$ , corresponding to (001), (111), and (312) crystal planes of various element phases in  $\text{MnO}_2$ , respectively. This result demonstrates that  $\text{MnO}_2$  is successfully attached to the surface of the MXene material [34–36]. Therefore, the successful synthesis of MXene/ $\text{MnO}_2$  composites is confirmed through the SEM and XRD pattern analyses.

### 3.2. Effect of Initial Concentration

According to Figure 3, the effect of MXene/ $\text{MnO}_2$  composites on the removal efficiency of U(VI) in solutions with different initial concentrations ranging from 10 to 200 mg/L was investigated. The results show that the adsorption capacity of MXene/ $\text{MnO}_2$  composites for U(VI) increases with the initial concentration of U(VI) in solutions up to 120 mg/L, achieving a removal efficiency of nearly 100%. The maximum adsorption capacity of MXene/ $\text{MnO}_2$  composites for U(VI) is 696 mg/g. However, when the initial concentration of U(VI) exceeds 120 mg/L, the adsorption capacity of the composite material decreases continuously. This phenomenon may be attributed to the exhaustion of active sites for reducing uranium atoms in the MXene/ $\text{MnO}_2$  composites at high initial concentrations of U(VI), leading to the saturation of the adsorption capacity. It may be because when the initial concentration of U(VI) solution keeps rising, the concentration of nitrate ( $\text{NO}_3^-$ ) also keeps rising because  $\text{UO}_2(\text{NO}_3)_2 \cdot 6\text{H}_2\text{O}$  is used, and MXene material will release  $\text{H}^+$  in the process of adsorption of U(VI), resulting in a slightly acidic solution. Under acidic conditions, the adsorption and removal of U(VI) by MXene/manganese dioxide composites will be hindered by nitrate, so the adsorption and removal capacity will continuously decrease at high initial concentration [37].



**Figure 3.** The effect of initial concentration of U(VI) on the removal of U(VI) from MXene/MnO<sub>2</sub> composites ( $T = 298$  K,  $pH = 7$ ).

### 3.3. Effect of pH

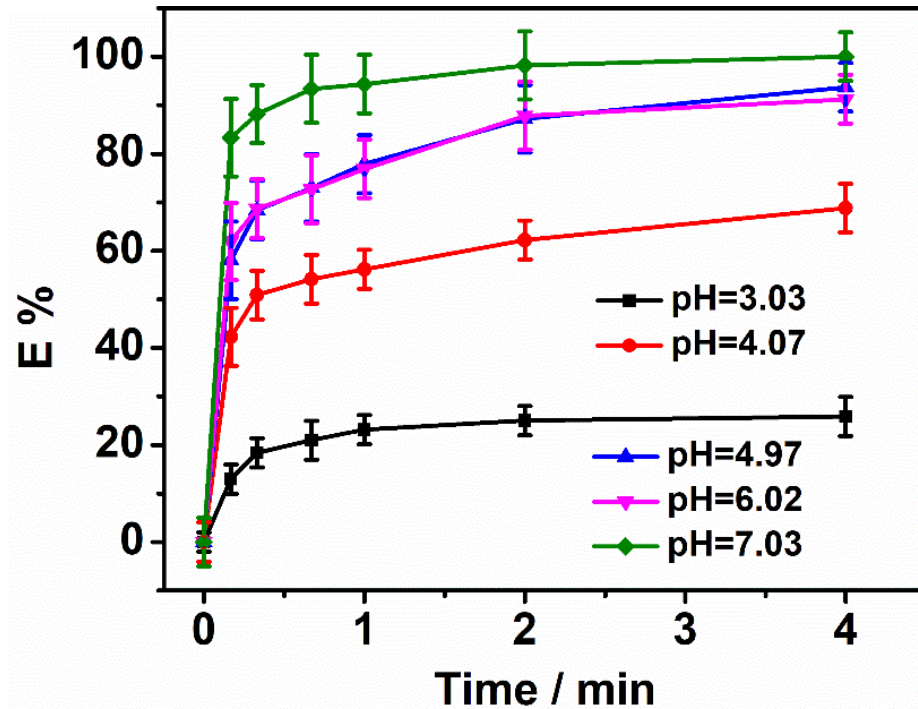
The effect of MXene/MnO<sub>2</sub> composites on the adsorption and removal efficiency of U(VI) with an initial concentration of 10 mg/L at different pH values is shown in Figure 4. In the U(VI) adsorption experiment, pH value has a significant effect on the adsorption reaction of the solution. The distribution of metal ions varies with the change in pH during solution adsorption, which also affects the surface charge distribution of composite materials. This will lead to changes in the surface active reduction sites of composites, which will have a significant impact on the adsorption reduction process. The adsorption reduction experiments were carried out at five pH conditions: 3.03, 4.07, 4.97, 6.02, and 7.03. The adsorption efficiency of the MXene/MnO<sub>2</sub> composites is only 20% when  $pH = 3.03$ , but the adsorption efficiency increases with the increase in pH. When  $pH = 4.97$  and  $6.02$ , the U(VI) removal rate reaches 90%, and when  $pH = 7.03$ , the U(VI) removal rate reaches nearly 100%. At lower pH values ( $pH = 3.03, 4.07$ ), uranium in U(VI) solution exists mainly in the form of hexavalent uranium, and most of it coexists in the form of uranyl ion ( $UO_2^{2+}$ ). However, under acidic conditions, such as at lower pH values, a large number of  $H^+$  ions will compete with  $UO_2^{2+}$  ions for adsorption [38]. In addition, protonation occurs on the surface of MXene/MnO<sub>2</sub> composites, resulting in positive surface charges under strongly acidic conditions. The positive charge will repel  $H^+$  ions, resulting in low adsorption efficiency at low pH. The MXene/MnO<sub>2</sub> composites were deprotonated at high pH, and the adsorption efficiency of U(VI) increased with the increase in pH value.

### 3.4. Effect of Coexisting Ions

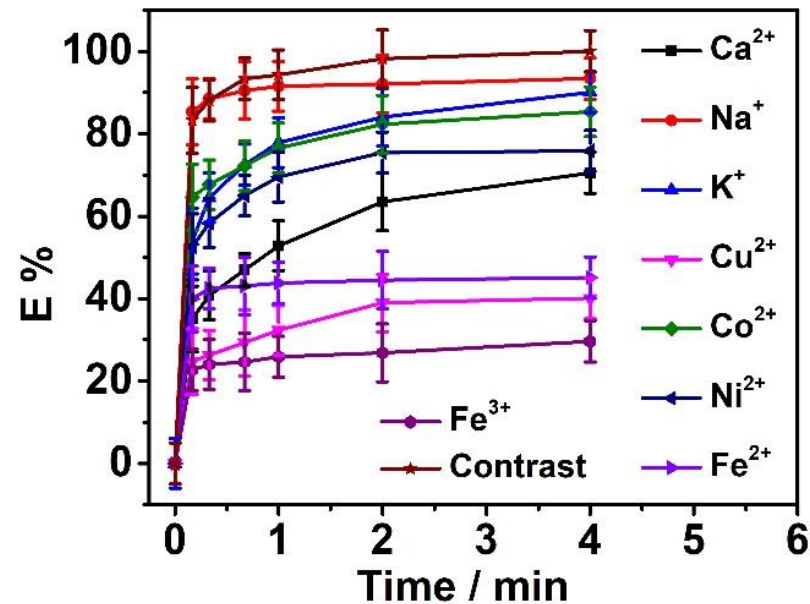
The removal of radioactive waste liquid involves not only uranyl ions but also other ions present in the waste. These coexisting ions can compete with uranyl ions for adsorption onto the MXene/MnO<sub>2</sub> composites, significantly affecting their adsorption efficiency. To elucidate the effects of different anions and cations, we performed the adsorption and reduction experiments of MXene/MnO<sub>2</sub> composites for U(VI) in the presence of eight competing cations and five anions.

Figure 5 shows the adsorption and removal efficiency of the MXene/MnO<sub>2</sub> composites for 10 mg/L U(VI) solution under the influence of different metal cations at room temperature ( $T = 298$  K). The results demonstrate that the MXene/MnO<sub>2</sub> composites are suitable for uranyl ion adsorption when there are  $Na^+$ ,  $K^+$ ,  $Co^{2+}$ ,  $Ni^{2+}$ , and  $Ca^{2+}$  ions, with an adsorption efficiency of above 70% and high removal efficiency. In particular, the composite material has a removal efficiency of over 90% for U(VI) in the presence of  $Na^+$ . However,

when the solution contains  $\text{Cu}^{2+}$ ,  $\text{Fe}^{2+}$ , and  $\text{Fe}^{3+}$  ions, the adsorption and removal efficiency of composite materials for uranium becomes lower, typically below 40%, with  $\text{Fe}^{3+}$  being only about 25%.



**Figure 4.** Effects of different pH values on the removal of U(VI) from the MXene/ $\text{MnO}_2$  composites ( $T = 298 \text{ K}$ ,  $\text{U(VI)} = 10 \text{ mg/L}$ ).



**Figure 5.** Effects of different cations on the removal of U(VI) from the MXene/ $\text{MnO}_2$  composites ( $T = 298 \text{ K}$ ,  $\text{U(VI)} = 10 \text{ mg/L}$ ).

These findings suggest that the MXene/ $\text{MnO}_2$  composites have strong selectivity for uranyl ion adsorption. While they exhibit lower selective adsorption for  $\text{K}^+$  and  $\text{Na}^+$  ions, they demonstrate higher adsorption capacities for  $\text{Cu}^{2+}$  and  $\text{Fe}^{3+}$  ions. However, in general, the adsorption capacity of MXene/ $\text{MnO}_2$  composites for U(VI) is the highest, possibly due to the difference in the density of the electron cloud between the uranyl ion and other metal

cations. Thus, the MXene/MnO<sub>2</sub> composites are preferred for uranyl ion adsorption over other metal cations.

Figure 6 shows the effects of different anions and acid ions on the adsorption of uranyl ions by MXene/MnO<sub>2</sub> composites at room temperature. The figure indicates that the presence of Cl<sup>-</sup> in the solution yields higher adsorption and removal efficiency of the uranyl ion, with an efficiency of 91.8%, while the presence of NO<sub>3</sub><sup>-</sup>, F<sup>-</sup>, SO<sub>4</sub><sup>2-</sup>, and HCO<sub>3</sub><sup>-</sup> leads to relatively lower adsorption efficiency, with an efficiency below 60%. This outcome may be due to the increase in solution acidity resulting from the release of H<sup>+</sup> from the [OH] functional group during the adsorption of uranyl ions in the MXene/MnO<sub>2</sub> composite. In a higher acid environment, other acid ions except for Cl<sup>-</sup> may inhibit the adsorption of uranyl ions by composite materials. Additionally, SO<sub>4</sub><sup>2-</sup> can form relatively stable complexes with uranyl ions, which are soluble in solution and therefore decrease the adsorption efficiency.

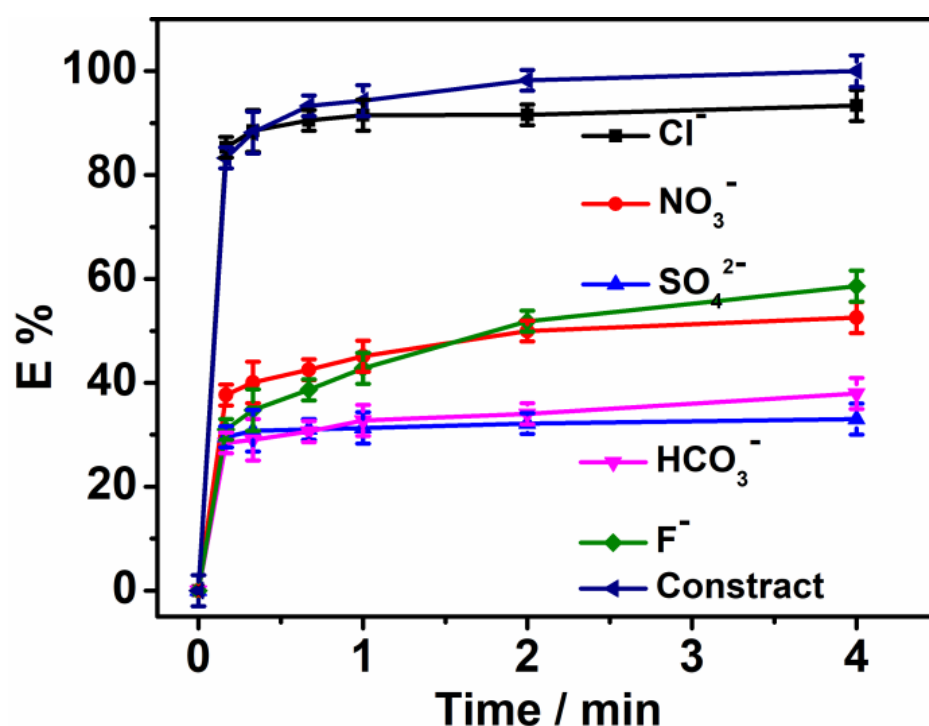


**Figure 6.** Effects of different anions on the removal of U(VI) from the MXene/MnO<sub>2</sub> composites (T = 298 K, U(VI) = 10 mg/L).

### 3.5. Effect of Humic Acid

The specific effect of humic acid on the adsorption of U(VI) by the MXene/MnO<sub>2</sub> composites was investigated by adding different concentrations of humic acid to the U(VI) solution. As shown in Figure 7, at room temperature, four concentrations of humic acid solutions (0.1 mg/L, 1 mg/L, 10 mg/L, and 20 mg/L) were tested to determine their effect on the adsorption of U(VI) by the composites. It can be observed from the figure that the removal efficiency E% of the uranyl ions gradually increases with a decrease in the concentration of humic acid. At a concentration of 20 mg/L, the removal efficiency is 60%, while at 0.1 mg/L, the removal efficiency reaches as high as 87%. Upon analysis, it is suggested that the decrease in adsorption efficiency with the increase in humic acid concentration could be attributed to the formation of a relatively stable complex between uranyl ions and humic acid in the solution. This complex is not easily adsorbed, which leads to a continuous decrease in adsorption efficiency. Humic acid contains various functional groups, such as carbonyl, carboxyl, or hydroxyl, which can make the uranyl ion in the solution more stable and can coordinate with the uranyl ion. Therefore, when the concentration of humic acid increases, the adsorption of U(VI) by the MXene/MnO<sub>2</sub>

composites is inhibited, although the final inhibition effect is not too strong [39,40]. Overall, these findings suggest that the MXene/MnO<sub>2</sub> composites have sufficient potential to remove natural ecological radionuclide uranium from wastewater in the environment.

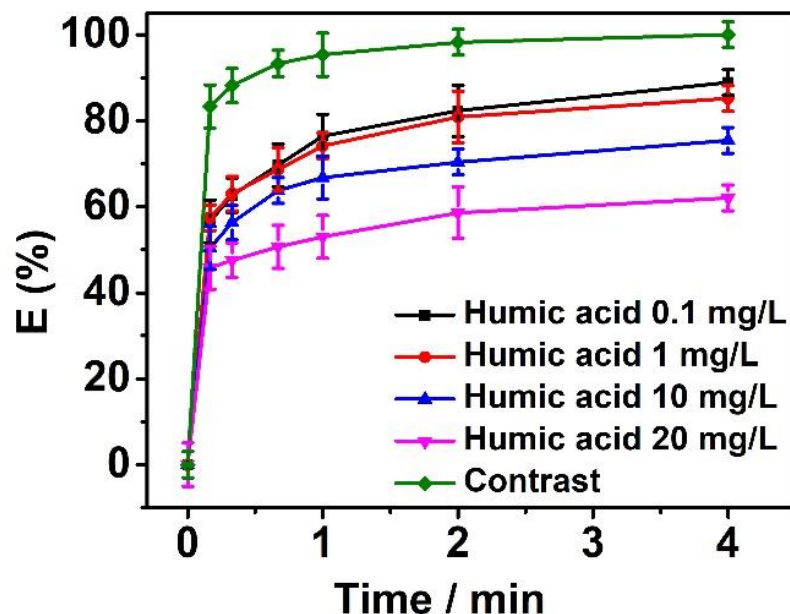


**Figure 7.** Effects of different humic acid concentrations on the removal of U(VI) from the MXene/MnO<sub>2</sub> composites (T = 298 K, U(VI) = 10 mg/L).

The potential mechanism of uranium removal by MXene/MnO<sub>2</sub> composites is yet to be investigated. Previous studies have confirmed that the O sites on MnO<sub>2</sub> can capture U(VI), while other oxygen-containing functional groups on the surface of MXene, such as Ti-O and C-O, also play an important role in the adsorption process [41]. As shown in Table 1.

**Table 1.** Uranium adsorption capacities by various materials including MXene and their composites [41–45].

Adsorbents	Initial [U(VI)]	pH	Adsorption Capacity (mg/g)	Ref.
Ti <sub>3</sub> C <sub>2</sub> T <sub>x</sub> -DMSO-hydrated	100 mg/L	5.0	214	[41]
Amidoxime-Functionalized Ti <sub>3</sub> C <sub>2</sub> T <sub>x</sub> Nanoflakes	21 mg/L	5.0	394	[42]
Fe/RGO composites	714 mg/L	6.5	4174	[43]
M-nZVI	100 mg/L	6.2	403.25	[44]
nZVI/Alk-Ti <sub>3</sub> C <sub>2</sub> T <sub>x</sub>	200 mg/L	3.5	1315	[45]
MXene/MnO <sub>2</sub>	120 mg/L	7.03	696	This work

Our results show that compared to previous studies reported [45], the MXene/MnO<sub>2</sub> composites exhibits a stronger ability to adsorb U(VI), indirectly indicating that MXene and MnO<sub>2</sub> can work together to promote uranium adsorption. Figure 8 provides a proposed mechanism for the adsorption of uranium by the MXene/MnO<sub>2</sub> composites.

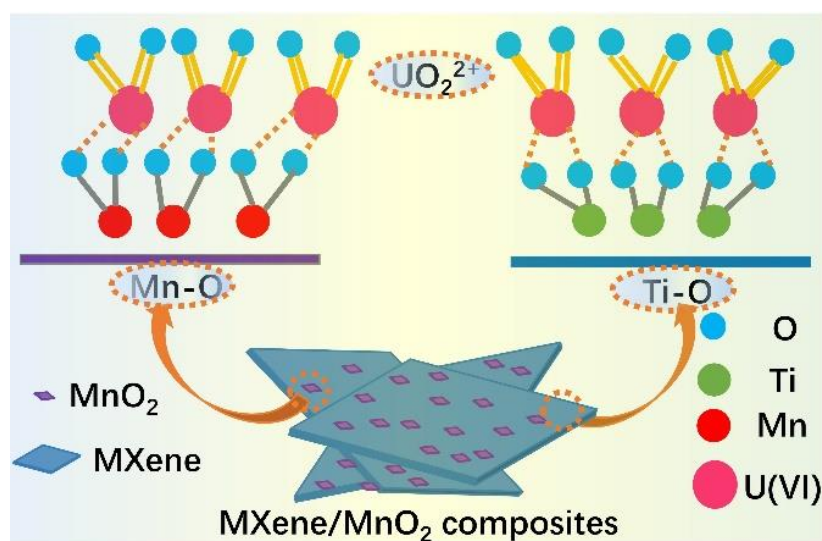


**Figure 8.** Possible adsorption mechanism of U(VI) by the MXene/MnO<sub>2</sub> composites.

#### 4. Conclusions

In conclusion, the U(VI) removal rate of the synthesized MXene/MnO<sub>2</sub> composites is up to 99%, and the maximum adsorption capacity is 696 mg/g. The composite material can reach adsorption equilibrium in just 4 min. Through experiments conducted under various environmental conditions, including different pH values, competitive cations and anions, and organic humic acid concentrations, it was found that the MXene/MnO<sub>2</sub> composite material exhibited strong selective ability for uranium adsorption and achieved high removal efficiencies of 91.2%, 69.7%, and 71.8% for U(VI) in the presence of various interfering factors. In conclusion, the MXene/MnO<sub>2</sub> composite material is a promising, effective, and environmentally friendly adsorbent for the removal of uranium from radioactive nuclear wastewater, which can help protect the environment.

**Author Contributions:** L.W. and Y.-L.L. contributed to the device design, data analysis, and writing. The material preparation and data collection were performed by Y.-L.L. All authors have read and agreed to the published version of the manuscript.

**Funding:** This work was financially supported by the start-up funding from University of South China (No. 220XQD016).

**Data Availability Statement:** All data generated or analyzed during this study are included in this article.

**Conflicts of Interest:** The authors declare no conflict of interest.

#### References

1. Dam, H.; Reinhoudt, D.; Verboom, W. Multicoordinate ligands for actinide/lanthanide separations. *Chem. Soc. Rev.* **2007**, *36*, 367–377. [[CrossRef](#)] [[PubMed](#)]
2. Ewing, R. Nuclear Fuel Cycle: Environmental Impact. *MRS Bull.* **2008**, *33*, 338–340. [[CrossRef](#)]
3. Schnug, E.; Lottermoser, B. Fertilizer-Derived Uranium and its Threat to Human Health. *Environ. Sci. Technol.* **2013**, *47*, 2433–2434. [[CrossRef](#)] [[PubMed](#)]
4. Li, Z.; Chen, F.; Yuan, L.; Liu, Y.; Zhao, Y.; Chai, Z.; Shi, W. Uranium(VI) adsorption on graphene oxide nanosheets from aqueous solutions. *Chem. Eng. J.* **2012**, *210*, 539–546. [[CrossRef](#)]
5. Yusan, S.; Akyil, S. Sorption of uranium(VI) from aqueous solutions by akaganeite. *J. Hazard. Mater.* **2008**, *160*, 388–395. [[CrossRef](#)]
6. Brandy, D.; Scott, F. Impact of Uranyl–Calcium–Carbonate Complexes on Uranium(VI) Adsorption to Synthetic and Natural Sediments. *Environ. Sci. Technol.* **2010**, *44*, 928–934.
7. Naguib, M.; Mashtalir, O.; Carle, J.; Presser, V.; Lu, J.; Hultman, L.; Gogotsi, Y.; Barsoum, M.W. Two-Dimensional Transition Metal Carbides. *ACS Nano* **2012**, *6*, 1322–1331. [[CrossRef](#)]
8. Peng, Q.; Guo, J.; Zhang, Q.; Xiang, J.; Liu, B.; Zhou, A.; Liu, R.; Tian, Y. Unique Lead Adsorption Behavior of Activated Hydroxyl Group in Two-Dimensional Titanium Carbide. *J. Am. Chem. Soc.* **2014**, *136*, 4113–4116. [[CrossRef](#)]

9. Charles, M.; Pascal, B.; Bernard, B. Separation of long-lived radionuclides from high active nuclear waste. *Comptes Rendus Phys.* **2002**, *3*, 797–811.
10. Bruno, J.; Ewing, R. Spent Nuclear Fuel. *Elements* **2006**, *2*, 343–349. [[CrossRef](#)]
11. Luo, X.; Zhang, G.; Wang, X. Research on a pellet co-precipitation micro-filtration process for the treatment of liquid waste containing strontium. *J. Radioanal. Nucl. Chem.* **2013**, *298*, 931–939. [[CrossRef](#)]
12. Xin, L. Study on Radioactive Wastewater Treatment by Precipitation and Membrane Separation. *Appl. Mech. Mater.* **2014**, *490–491*, 972–975.
13. Abdi, S.; Nasiri, M.; Mesbahi, A.; Khani, M.h. Investigation of uranium (VI) adsorption by polypyrrole. *J. Hazard. Mater.* **2017**, *332*, 132–139. [[CrossRef](#)] [[PubMed](#)]
14. Sureshkumar, M.K.; Das, D.; Mallia, M.B.; Gupta, P.C. Adsorption of uranium from aqueous solution using chitosan-tripolyphosphate (CTPP) beads. *J. Hazard. Mater.* **2010**, *184*, 65–72. [[CrossRef](#)] [[PubMed](#)]
15. Amesh, P.; Venkatesan, K.A.; Suneesh, A.S.; Samanta, N. Diethylenetriamine tethered mesoporous silica for the sequestration of uranium from aqueous solution and seawater. *J. Environ. Chem. Eng.* **2020**, *8*, 103995. [[CrossRef](#)]
16. Gan, J.; Zhang, L.; Wang, Q.; Xin, Q.; Hu, E.; Lei, Z.; Wang, H.; Wang, H. Synergistic action of multiple functional groups enhanced uranium extraction from seawater of porous phosphorylated chitosan/coal-based activated carbon composite sponge. *Desalination* **2023**, *545*, 116154. [[CrossRef](#)]
17. Parab, H.; Joshi, S.; Shenoy, N.; Verma, R.; Lali, A.; Sudersanan, M. Uranium removal from aqueous solution by coir pith: Equilibrium and kinetic studies. *Bioresour. Technol.* **2005**, *96*, 1241–1248. [[CrossRef](#)]
18. Wang, G.; Liu, J.; Wang, X.; Xie, Z.; Deng, N. Adsorption of uranium (VI) from aqueous solution onto cross-linked chitosan. *J. Hazard. Mater.* **2009**, *168*, 1053–1058. [[CrossRef](#)]
19. Yan, T.; Luo, X.; Zou, Z.; Lin, X.; He, Y. Adsorption of Uranium(VI) from a Simulated Saline Solution by Alkali-Activated Leather Waste. *Ind. Eng. Chem. Res.* **2017**, *56*, 3251–3258. [[CrossRef](#)]
20. Liu, Y.-L.; Wang, L.; Zeng, Q.; Yan, C.; Kang, Q. A homologous strategy to parallelly construct doped MOFs-derived electrodes for flexible solid-state hybrid supercapacitors. *Nano Res.* **2023**. [[CrossRef](#)]
21. Shang, J.; Liu, C.; Wang, Z.; Zachara, J.M. Effect of Grain Size on Uranium(VI) Surface Complexation Kinetics and Adsorption Additivity. *Environ. Sci. Technol.* **2011**, *45*, 6025–6031. [[CrossRef](#)] [[PubMed](#)]
22. Yu, J.; Yu, C.; Zhu, W.; He, G.; Wei, Y.; Zhou, J. Hydrous titanium oxide and bayberry tannin co-immobilized nano collagen fibrils for uranium extraction from seawater and recovery from nuclear wastewater. *Chemosphere* **2021**, *286*, 131626. [[CrossRef](#)] [[PubMed](#)]
23. Yan, C.; Liu, Y.-L.; Zeng, Q.; Wang, G.-G.; Han, J. 2D Nanomaterial Supported Single-Metal Atoms for Heterogeneous Photo/Electrocatalysis. *Adv. Funct. Mater.* **2023**, *33*, 2210837. [[CrossRef](#)]
24. Othman, Z.; Mackey, H.R.; Mahmoud, K.A. A critical overview of MXenes adsorption behavior toward heavy metals. *Chemosphere* **2022**, *295*, 133849. [[CrossRef](#)]
25. Zhang, Y.; Zhou, J.; Wang, D.; Cao, R.; Li, J. Performance of MXene incorporated MOF-derived carbon electrode on deionization of uranium(VI). *Chem. Eng. J.* **2022**, *430*, 132702. [[CrossRef](#)]
26. Wang, D.; Song, J.; Wen, J.; Yuan, Y.; Liu, Z.; Lin, S.; Wang, H.; Wang, H.; Zhao, S.; Zhao, X. Significantly Enhanced Uranium Extraction from Seawater with Mass Produced Fully Amidoximated Nanofiber Adsorbent. *Adv. Energy Mater.* **2018**, *8*, 1802607. [[CrossRef](#)]
27. Ma, L.; Huang, Y.; Deng, H.; Yin, H.; Tian, Q.; Yan, M. Removal of Uranium (VI) from Acidic Aqueous Solution by Fluorapatite. *J. Inorg. Mater.* **2021**, *37*, 395–403. [[CrossRef](#)]
28. Yu, R.; Lu, Y.; Zhang, X.; Chen, W.; Chen, X.; Li, L. Amidoxime-modified ultrathin polyethylene fibrous membrane for uranium extraction from seawater. *Desalination* **2022**, *539*, 115965. [[CrossRef](#)]
29. Zhou, Z.; Liu, Q.; Zhu, J.; Liu, J.; Zhang, H.; Yu, J.; Chen, R.; Li, Y.; Wang, J. Defective carbon nitride ultrathin nanosheets enriched with amidoxime groups for enhanced visible light-driven reduction of hexavalent uranium. *J. Colloid Interface Sci.* **2022**, *628*, 840–848. [[CrossRef](#)]
30. Sun, Y.; Li, Y. Application of surface complexation modeling on adsorption of uranium at water-solid interface: A review. *Environ. Pollut.* **2021**, *278*, 116861. [[CrossRef](#)]
31. Xiao, F.; Cheng, Y.; Zhou, P.; Chen, S.; Wang, X.; He, P.; Nie, X.; Dong, F. Fabrication of novel carboxyl and amidoxime groups modified luffa fiber for highly efficient removal of uranium(VI) from uranium mine water. *J. Environ. Chem. Eng.* **2021**, *9*, 105681. [[CrossRef](#)]
32. Yang, A.-L.; Yang, S.-Y.; Zhu, Y.-K. Magnetic modification of used tea leaves for uranium adsorption. *New Carbon Mater.* **2021**, *36*, 821–826. [[CrossRef](#)]
33. Zeng, J.; Zhang, H.; Sui, Y.; Hu, N.; Ding, D.; Wang, F.; Xue, J.; Wang, Y. New Amidoxime-Based Material TMP-g-AO for Uranium Adsorption under Seawater Conditions. *Ind. Eng. Chem. Res.* **2017**, *56*, 5021–5032. [[CrossRef](#)]
34. Chen, X.; Wang, Y.; Lv, J.; Feng, Z.; Liu, Y.; Xia, H.; Li, Y.; Wang, C.; Zeng, K.; Liu, Y.; et al. Simple one-pot synthesis of manganese dioxide modified bamboo-derived biochar composites for uranium(vi) removal. *New J. Chem.* **2022**, *46*, 14427–14438. [[CrossRef](#)]
35. Wen, D.; Ying, G.; Liu, L.; Sun, C.; Li, Y.; Zhao, Y.; Ji, Z.; Wu, Y.; Zhang, J.; Zhang, J.; et al. Flexible and High-Performance MXene/MnO<sub>2</sub> Film Electrodes Fabricated by Inkjet Printing: Toward a New Generation Supercapacitive Application. *Adv. Mater. Interfaces* **2021**, *8*, 2101453. [[CrossRef](#)]

36. Wang, Q.; Zhang, Z.; Zhang, Z.; Zhou, X.; Ma, G. Facile synthesis of MXene/MnO<sub>2</sub> composite with high specific capacitance. *J. Solid State Electrochem.* **2019**, *23*, 361–365. [[CrossRef](#)]
37. Zhong, L.; He, F.; Liu, Z.; Dong, B.; Ding, J. Adsorption of uranium (VI) ions from aqueous solution by acrylic and diaminomaleonitrile modified cellulose. *Colloids Surf. A Physicochem. Eng. Asp.* **2022**, *641*, 128565. [[CrossRef](#)]
38. Zhang, P.; Wang, L.; Du, K.; Wang, S.; Huang, Z.; Yuan, L.; Li, Z.; Wang, H.; Zheng, L.; Chai, Z.; et al. Effective removal of U(VI) and Eu(III) by carboxyl functionalized MXene nanosheets. *J. Hazard. Mater.* **2020**, *396*, 122731. [[CrossRef](#)]
39. Yao, W.; Wu, Y.; Pang, H.; Wang, X.; Yu, S.; Wang, X. In-situ reduction synthesis of manganese dioxide@polypyrrole core/shell nanomaterial for highly efficient enrichment of U(VI) and Eu(III). *Sci. China Chem.* **2018**, *61*, 812–823. [[CrossRef](#)]
40. Li, K.; Xiong, T.; Liao, J.; Lei, Y.; Zhang, Y.; Zhu, W. Design of MXene/graphene oxide nanocomposites with micro-wrinkle structure for efficient separating of uranium(VI) from wastewater. *Chem. Eng. J.* **2022**, *433*, 134449. [[CrossRef](#)]
41. Wang, L.; Tao, W.; Yuan, L.; Liu, Z.; Huang, Q.; Chai, Z.; Gibson, J.K.; Shi, W. Rational control of the interlayer space inside two-dimensional titanium carbides for highly efficient uranium removal and imprisonment. *Chem. Commun.* **2017**, *53*, 12084–12087. [[CrossRef](#)] [[PubMed](#)]
42. Zhang, P.; Wang, L.; Huang, Z.; Yu, J.; Li, Z.; Deng, H.; Yin, T.; Yuan, L.-Y.; Gibson, J.K.; Mei, L.; et al. Aryl Diazonium-Assisted Amidoximation of MXene for Boosting Water Stability and Uranyl Sequestration via Electrochemical Sorption. *ACS Appl. Mater. Interfaces* **2020**, *12*, 15579–15587. [[CrossRef](#)] [[PubMed](#)]
43. Li, Z.-J.; Wang, L.; Yuan, L.-Y.; Xiao, C.-L.; Mei, L.; Zheng, L.-R.; Zhang, J.; Yang, J.-H.; Zhao, Y.-L.; Zhu, Z.-T.; et al. Efficient removal of uranium from aqueous solution by zero-valent iron nanoparticle and its graphene composite. *J. Hazard. Mater.* **2015**, *290*, 26–33. [[CrossRef](#)] [[PubMed](#)]
44. Xu, J.; Li, Y.; Jing, C.; Zhang, H.; Ning, Y. Removal of uranium from aqueous solution using montmorillonite-supported nanoscale zero-valent iron. *J. Radioanal. Nucl. Chem.* **2014**, *299*, 329–336. [[CrossRef](#)]
45. Wang, S.; Wang, L.; Li, Z.; Zhang, P.; Du, K.; Yuan, L.; Ning, S.; Wei, Y.; Shi, W. Highly efficient adsorption and immobilization of U(VI) from aqueous solution by alkalized MXene-supported nanoscale zero-valent iron. *J. Hazard. Mater.* **2021**, *408*, 124949. [[CrossRef](#)] [[PubMed](#)]

**Disclaimer/Publisher's Note:** The statements, opinions and data contained in all publications are solely those of the individual author(s) and contributor(s) and not of MDPI and/or the editor(s). MDPI and/or the editor(s) disclaim responsibility for any injury to people or property resulting from any ideas, methods, instructions or products referred to in the content.